RSC Advances

ROYAL SOCIETY OF CHEMISTRY

www.rsc.org/advances

Journal Name

ARTICLE

Solution processable low bandgap thienoisoindigo-based small molecules for organic electronic devices †

Received 00th January 20xx,
Accepted 00th January 20xx

DOI: 10.1039/x0xx00000x

www.rsc.org/

Pei Han[a], Xiaohui Gong[a], Baoping Lin*[a], Zhenhong Jia[b], Shanghui Ye*[b], Ying Sun[a], Hong Yang[a]

Two donor-acceptor conjugated small molecules that consist of thienoisoindigo as an acceptor unit and benzofuran or naphthalene as donor building block have been synthesized via Suzuki coupling reaction. The small molecules, TII(BFu)$_2$ and TII(Na)$_2$, exhibit broad and near-infrared absorption in the range of 500-900 nm while their absorption maxima locate at around 620 nm in films. Optical band gaps calculated from the solid state absorption cutoff value are 1.49 eV for TII(BFu)$_2$ and 1.53 eV for TII(Na)$_2$, respectively. These small molecules possess p-channel charge transport characteristics when used as the active semiconductor in organic thin-film transistors (OFETs). The highest hole mobility of 1.28×10^{-3} cm^2 V^{-1} s^{-1} for TII(BFu)$_2$ and 1.29×10^{-3} cm^2 V^{-1} s^{-1} for TII(Na)$_2$ have been achieved in top-contact-bottom-gate OFET devices . The preliminary characterization of bulk heterojunction photovoltaic devices consisting of the small molecules and PC$_{71}$BM yield power conversion efficiencies (PCE) of 1.24% for TII(BFu)$_2$ and 1.04% for TII(Na)$_2$. Moreover, the relationships between the semiconductor devices performance and film morphology, energy levels are discussed.

Introduction

Solution-processable donor-acceptor (D-A) type conjugated small molecule and polymer organic semiconductors have attracted extensive attention as active materials in organic field effect transistors (OFETs) [1-3] and organic photovoltaics (OPVs) [4-6] over the last decade. Compared to polymers, small molecule materials have the advantages of simple synthesis and purification as well-defined structures, thus eliminating the batch-to-batch variation in device fabrication [5]. Therefore, a large number of small molecular materials have been studied for OFET and OPV applications [7-12]. Till now, small molecules based OPV devices have exhibited power conversion efficiency (PCE) as high as 9.3% [13].

Recently, the donor-acceptor (D-A) type organic semiconductor materials have been extensively investigated for OFETs and OPV devices because they have the advantages of wide absorption spectrum from UV-vis to NIR regions, controllable energy levels and band gap tuning. Diketopyrrolopyrrole (DPP) [14-16] and isoindigo (II) [17, 18] have been researched as electron-deficient building blocks for making D-A type semiconductor materials due to their excellent performances in OFETs and OPV devices. Very recently, a new series of D-A type small molecules and polymers based on thienoisoindigo (TII) have been synthesized , and applied in OFETs and OPV devices [19-23]. TII structure is thienopyrrolone units by replacing the benzene rings of II with thiophenes, which might further enhance planarity along the backbone and promote intermolecular π-π interactions by the further effective conjugation. The TII based conjugated polymer with naphthalene unit has been reported as OFET material with high hole mobility of 14.4 cm^2 V^{-1} s^{-1} [24].

Herein, we present two TII-based D-A-D type small molecule materials synthesized with electron-donor units such as benzofuran or naphthalene (abbreviated as TII(BFu)$_2$ and TII(Na)$_2$, see Fig. 1 for their molecular structures), and explore their semiconducting properties. The highest hole mobility of 1.28×10^{-3} cm^2 V^{-1} s^{-1} for TII(BFu)$_2$ and 1.29×10^{-3} cm^2 V^{-1} s^{-1} for TII(Na)$_2$ were achieved in top-contact-bottom-gate OFETs. We further investigated the OPV

[a] School of Chemistry and Chemical Engineering, Southeast University, Nanjing 211189, PR China.
E-mail: lbp@seu.edu.cn
[b] Key Laboratory for Organic Electronics & Information Displays (KLOEID) and Institute of Advanced Materials (IAM), Nanjing University of Posts & Telecommunications, Nanjing 210046, PR China.
E-mail: yeshh@iccas.ac.cn

† Electronic Supplementary Information (ESI) available: ^{1}H and ^{13}C NMR spectra, electrochemical and OFET data. See DOI: 10.1039/x0xx00000x

Fig. 1. Chemical structures of TII(BFu)$_2$ and TII(Na)$_2$.

performances based on these small molecules as donor material and $PC_{71}BM$ as acceptor material, which showed the best PCE of 1.24% for $TII(BFu)_2$ and 1.04% for $TII(Na)_2$.

Results and discussion

The synthetic routes for the conjugated small molecules ($TII(BFu)_2$ and $TII(Na)_2$) are summarized in Fig. 2. Although several different ways are possible to synthesize thienoisoindigo structure, route shown in Fig. 2 was selected owing to its convenient synthetic methods and mild reaction conditions. Based on published procedures[19, 20], the alkylated thiophene-3-amine monomer 2 was prepared from commercially available 3-bromothiophene and dodecylamine. Followed by a cylization of monomer 2 with oxalyl chloride, the thiophene anologue of isatin 3 was obtained. The key material thienoisoindigo (TII) was successfully synthesized by the dimerization of compound 3 with Lawesson's reagent. After bromination with NBS, $TII(BFu)_2$ and $TII(Na)_2$ were synthesized through Suzuki coupling reactions from benzofuran-2-boronic acid and naphthalene-2-ylboronic acid using $Pd(PPh_3)_4$ as the catalyst. Two molecules are readily soluble in chloroform, chlorobenzene and o-dichlorobenzene and form uniform thin films by spin coating.

Thermal analyses of the small molecules were carried out by thermogravimetric analysis (TGA). The TGA revealed good thermal stability of these small molecules with decomposition temperature at 5% weight loss exceeding 392 ºC ($TII(BFu)_2$) and 393 ºC ($TII(Na)_2$) respectively, indicating that these small molecules are thermally stable (Fig. 3).

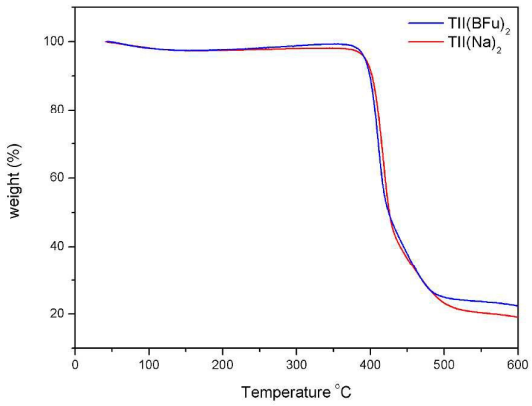

Fig. 3. TGA curves of $TII(BFu)_2$ and $TII(Na)_2$.

The optical properties of $TII(BFu)_2$ and $TII(Na)_2$, both in chloroform solution and thin films, were studied by UV-vis absorption spectroscopy and are shown in Fig. 4. The UV spectrum of $TII(BFu)_2$ and $TII(Na)_2$ in chloroform exhibited a broad absorption band with a maxima (λ_{max}) at 650 nm and 633 nm respectively, which corresponds to the intramolecular charge transfer (ICT) transition. The 17 nm red shift in λ_{max} observed for the $TII(BFu)_2$ compared to $TII(Na)_2$ is due to the strong donor-acceptor interactions between benzofuran and TII moiety. The film absorption spectra of both small molecules were quite broader and exhibited a slight blue shift compared to the solution spectra. The optical band gaps for $TII(BFu)_2$ and $TII(Na)_2$ were calculated from the absorption cutoff value in the solid state and were found to be 1.49 eV and 1.53 eV respectively (Table 1).

The HOMO and LUMO energy levels were studied by cyclic voltammetry (CV), as shown in Fig. 5 and Fig. S12, and the results are summarized in Table 1. These energy levels are critical to the functioning of OFET and OPV devices. The HOMO values were calculated with reference to the ferrocene oxidation onset potential according HOMO = - $(4.4+E_{oxd,onset})$ (eV) equation. Using Ag/AgCl as the reference electrode, the oxidation onset potential of $TII(BFu)_2$ and $TII(Na)_2$ are 0.69 and 0.66 V, respectively, from Fig 5. Then HOMO energy levels can be calculated as -5.09 and -5.06 eV for $TII(BFu)_2$ and $TII(Na)_2$. The LUMO levels were derived as -3.60 and -3.53 eV from the HOMO levels and optical band gaps of each compound.

In order to futher study the electrochemical properties of $TII(BFu)_2$ and $TII(Na)_2$, density functional theory (DFT) calculations using the Gaussian 03 program based on the B3LYP/6-31G(d) have been performed. To expedite the calculation, model compounds with methyl groups replacing the alkyl chains on the TII nitrogen. Fig. 6 shows the simulated energy levels of the frontier orbitals, theirsurface plots, and geometric models of their structures. The model molecular geometries of $TII(BFu)_2$ are almost flat, while the torsinal angle of $TII(Na)_2$ between naphene ring and thienoindigo unit is 24.5°. The calculated HOMO and LUMO energies of the ground-state optimized geometry of $TII(BFu)_2$ and $TII(Na)_2$ are -5.16/-5.15 eV and -3.51/-3.38 eV, respectively (fitted data according

Fig. 2. Synthetic schemes of $TII(BFu)_2$ and $TII(Na)_2$. Reagents and conditions: (i) dodecylamine, Cu/CuI, K_3PO_4, dimethl ethanolamine, 85 °C, 41.3%; (ii) oxalyl dichloride, Et_3N, CH_2Cl_2, 0 °C, 68.1%; (iii) Lawesson's reagent, toluene, 65 °C, 34.4%; (iv) NBS, THF, r.t., 78.7%; (v) benzofuran-2-boronic acid or 2-naphthyl boronic acid, $Pd(PPh_3)_4$, toluene, aqueous K_2CO_3 solution (2 M), 90 °C, for $TII(BFu)_2$, 69.2%; for $TII(Na)_2$, 74.6%.

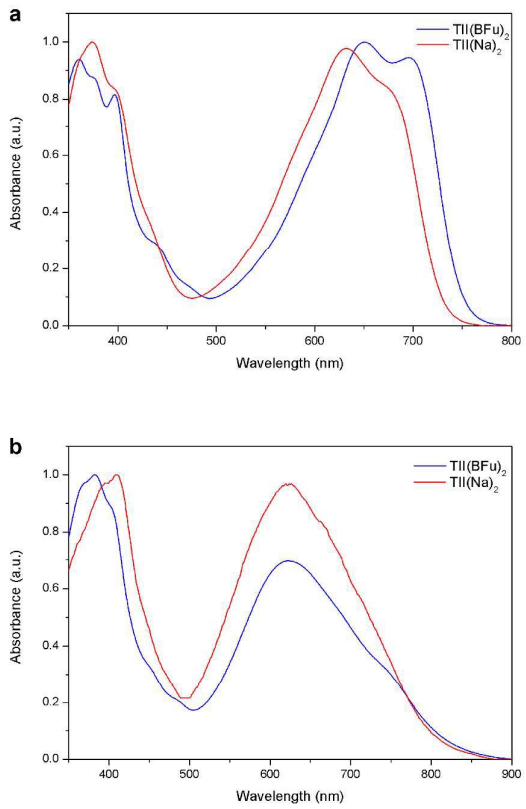

Fig. 4. UV-vis absorption spectra of $TII(BFu)_2$ and $TII(Na)_2$ (a) in chloroform solution and (b) in solid thin films.

reference[25]). The results from the DFT calculations agree quite well with those derived from the UV-vis and the cyclic voltammograms.

Top-contact-bottom-gate OFET devices with $TII(BFu)_2$ and $TII(Na)_2$ active channel layers were fabricated by spin coating semiconductor layers approximately 40 nm thick onto highly p-doped Si with a 200 nm layer of thermally grown SiO_2 dielectric layer that was pretreated with octyl trichlorosilane (OTS).

The active films were annealed at various temperatures (ranging from 110 to 170 °C) on a hot plate under a nitrogen atmosphere for 10 min before gold source and drain electrodes were thermally evaporated through shadow masks. The typical channel length and width of devices were 80 μm and 8800 μm, respectively. Both $TII(BFu)_2$ and $TII(Na)_2$ exhibited p-channel characteristics. The output and transfer curves of $TII(BFu)_2$ and $TII(Na)_2$ based OTFTs are shown in Fig. 7, Fig. S13 and Fig. S14. The hole mobility values of these devices were calculated from the saturation regime of the transfer curves.

The highest hole mobility is 1.28×10^{-3} cm^2 V^{-1} s^{-1} for $TII(BFu)_2$ annealed at 130 °C, and 1.29×10^{-3} cm^2 V^{-1} s^{-1} for $TII(Na)_2$ annealed at 150 °C. The I_{on}/I_{off} ratio, threshold voltage (V_{th}) and mobility values at various annealing temperature have been listed in Table 2. Almost similar hole mobility values for both small molecules are possible due to the nearly identical HOMO energy levels, despite the effect of different electron donor units and the difference of the dihedral angle between the thienoisoindigo unit and the donor unit. These hole mobility values are one order of magnitude larger than those of the analogues with DPP or II structures, and are comparable with those of the thienoisoindigo materials reported recently[16, 18]. Furthermore, the significant increase in hole mobility after annealing is due to the slight increment in the crystallinity of the active layer thin films. This has been confirmed by atomic force microscopy (AFM) below.

The morphological behaviour of $TII(BFu)_2$ and $TII(Na)_2$ were investigated by tapping-mode atomic force microscopy (AFM) using spin coated thin films (similar to the device fabrication conditions) on Si/SiO_2 substrates. Fig. 8 displays the height images of the films annealed at 130 °C for $TII(BFu)_2$ and 150 °C for $TII(Na)_2$, respectively. AFM images of both small molecule pre-annealed films exhibit large crystalline domains, which are beneficial for field-effect hole mobility. The root-mean-square (RMS) roughness of $TII(BFu)_2$ and $TII(Na)_2$ films are 11.1 nm and 14.9 nm,

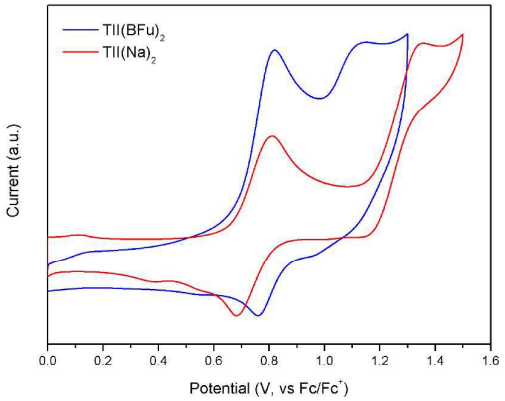

Fig. 5. Cyclic voltammograms of $TII(BFu)_2$ and $TII(Na)_2$ in CH_2Cl_2 containing 0.1 M tetrabutylammonium perchlorate; scan rate: 0.1 V s^{-1}.

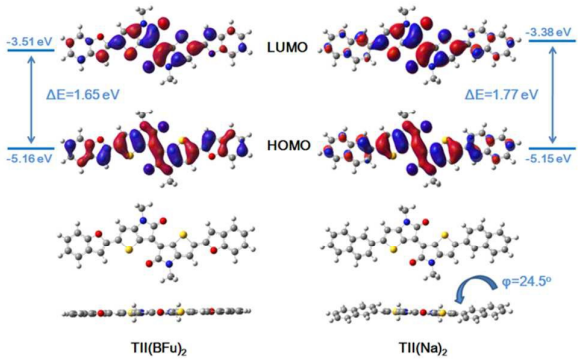

Fig. 6. Optimized molecular geometries, HOMO/LUMO surface plots and energy levels for model molecules calculated by Gaussian 03 program.

Table 1 Electrochemical and optical data of thienoisoindigo compounds.

Compounds	λ_{max} (nm)		E_g^{opt} [a] (eV)	HOMO[b] (eV)	LUMO[c] (eV)
	Solution	Film			
TII(BFu)$_2$	359, 397, 650, 695	382, 621	1.49	-5.09	-3.60
TII(Na)$_2$	373, 633	409, 623	1.53	-5.06	-3.53

[a] Estimated from the absorption edge of the films, E_g^{opt}=1240/λ_{onset}.

[b] HOMO levels were calculated according to following equation: HOMO = -(4.4+$E_{oxd,onset}$) (eV).

[c] LUMO levels derived from E_{HOMO} and E_g^{opt} of thienoisoindigo compounds.

respectively.

Due to wide absorption in the UV-vis-NIR region, appropriate HOMO and LUMO energy levels, and hole mobility characteristics of TII(BFu)$_2$ and TII(Na)$_2$, we used them as an electron donor in combination with $PC_{71}BM$ as an electron acceptor for the fabrication of conventional bulk-heterojunction photovoltaic solar cells (ITO/PEDOT:PSS/active layer/Al). The active layers were applied by spin coating from the chloroform solution, where the total concentration of the donor and acceptor materials was 10 mg mL^{-1}, and annealed at 130 ^{o}C for 10 min to optimize the device performance. The current density-voltage (J-V) characteristics of the OPV devices under simulated AM1.5 illumination are shown in Fig. 9 and corresponding photovoltaic parameters are summarized in Table 2. These photovoltaic devices show the best PCE of 1.24% for TII(BFu)$_2$ and 1.04% for TII(Na)$_2$. Both TII(BFu)$_2$ and TII(Na)$_2$ give the best OPV performance when donor/acceptor weight ratio was optimized to be 1:1 to achieve balanced charge carrier transport. As expected these two small molecules give lower V_{oc} (0.74 V for TII(BFu)$_2$ and 0.66 V for TII(Na)$_2$) than that analogues based on DPP due to their lower oxidation potential, whereas these values are comparable with other TII structures reported recently. Taking advantage of the high hole mobility, both small molecules afford a high fill factor (FF) 0.65 for TII(BFu)$_2$ and 0.49 for TII(Na)$_2$,

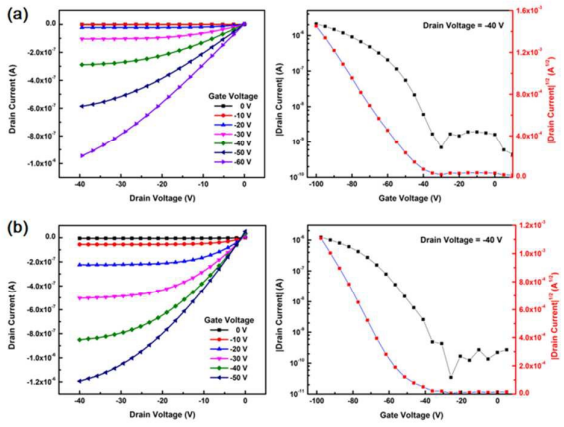

Fig. 7. Output (left) and transfer (right) characteristics for (a) TII(BFu)$_2$ film pre-annealed at 130 ^{o}C and (b) TII(Na)$_2$ film pre-annealed at 150 ^{o}C.

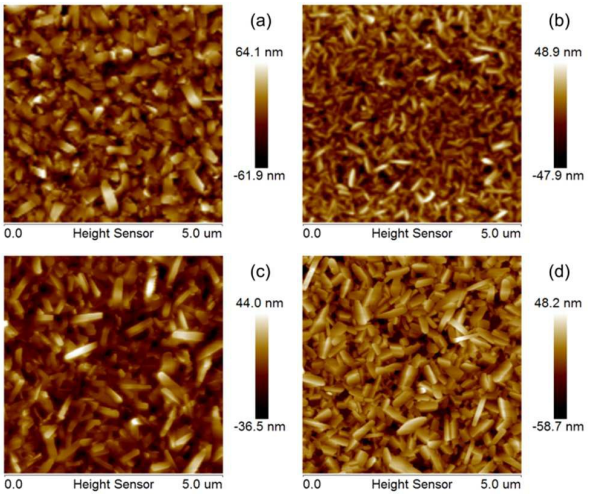

Fig. 8. AFM height images of TII(BFu)$_2$ (a), TII(Na)$_2$ (b) thin films without annealing (room temperature) and annealed at 130 ^{o}C for TII(BFu)$_2$ (c), 150 ^{o}C for TII(Na)$_2$ (d) on Si/SiO_2 substrates.

respectively.

Conclusions

In summary, we have synthesized two new TII-based D-A-D type small molecule materials (TII(BFu)$_2$ and TII(Na)$_2$) through the Suzuki coupling reaction. The stronger acceptor character of the TII unit broadened the absorption spectrum of the small molecules to longer wavelengths and resulted in low band gaps, relative to the analogue compounds with DPP or II structure. The OFET results showed that the two small molecules have hole mobilieties as high as 1.28×10^{-3} cm^2 V^{-1} s^{-1} for TII(BFu)$_2$ and 1.29×10^{-3} cm^2 V^{-1} s^{-1} for TII(Na)$_2$. Moreover, the photovoltaic properties of the small

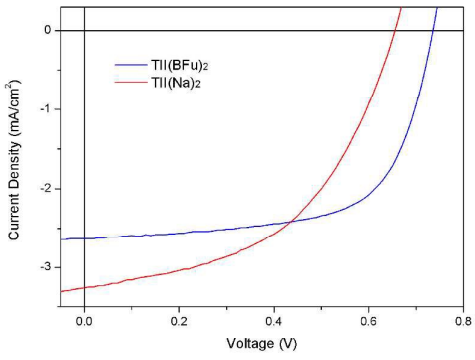

Fig. 9. Current density-votage (J-V) curves of TII(BFu)$_2$ or TII(Na)$_2$:$PC_{71}BM$ (1:1 w/w, thermally annealed at 130 ^{o}C for 10 min) BHJ solar cells under AM 1.5G illumination, 100 mW cm^{-2}.

Table 2 Organic field transistor (OFET) and photovoltaic (OPV) device characteristics.

Compounds	OFET characteristics			OPV characteristics			
	$I_{on/off}$	V_{th} (V)	μ_h ($cm^2V^{-1}s^{-1}$)	V_{oc} (V)	J_{sc} (mA cm^{-2})	FF	PCE (%)
$TII(BFu)_2$	10^4	-38	1.28×10^{-3}	0.74	2.61	0.65	1.24
$TII(Na)_2$	10^5	-48	1.29×10^{-3}	0.66	3.23	0.49	1.04

molecules were investigated and achieved the highest PCEs 1.24% for $TII(BFu)_2$ and 1.04% for $TII(Na)_2$, respectively. Further attempt to improve the semiconductor properties of TII based small molecules as well as molecular design is underway in our laboratory.

Experimental

General

All reactions involving air-sensitive reagents were performed under dry nitrogen. Reagent grade anhydrous tetrahydrofuran (THF) was freshly distilled over Na/benzophenone under nitrogen prior to use. Toluene was distilled over calcium hydride under nitrogen prior to use. All the other starting materials were purchased commercially and used without further purification, unless otherwise stated.

^1H and ^{13}C NMR measurements were carried out on a Bruker HW500 MHz spectrometer (AVANCE AV-500) or a Bruker HW300 MHz spectrometer (AVANCE AV-300) with tetramethylsilane (TMS) as the internal reference. Mass Spectometry (MS) data were obtained on a Bruker Daltonics BIFLEX III MALDI-TOF Analyzer using MALDI mode. High resolution mass spectra (HRMS) were recorded with a Bruker maxis mass spectrometer. Elemental analyses were carried out using a Vario EL CHNS elemental analyzer. The UV-vis absorption spectra were obtained by using an ultraviolet spectrophotometer (UV-3600, Japan). Thermogravimetric analysis (TGA) measuiments were collected using a Thermogravimetric Analyzer (STA 409) under a heating rate of 10 ^oC min^{-1} and a nitrogen flow of 100 mL min^{-1}. Cyclic voltammetry was performed on a CHI800C electrochemical workstation (Shanghai, China) with a three-electrode cell in dichloromethane with 0.1 M of tetrabutylammonium perchlorate using platinum electrodes at a scan rate of 100 mV s^{-1} and Ag/AgCl as the reference electrode, the Fc^+/Fc couple was used as te internal standard. The film surface morphology was measured with AFM (Seiko Instruments, SPA-400). DFT calculations were performed using the Gaussian 03 program package. The calculation was optimized at the B3LYP/6-31G(d) level of theory. The molecular orbitals were visualized using Gaussview[26].

Device fabrication and characterization

OFET devices. Top-contact-bottom-gate OFET test devices were fabricated using heavily p-doped silicon wafer (the gate) with a 200 nm layer of thermally grown SiO_2 dielectric (capacitance (C_i) of 18 nF cm^{-2}). The SiO_2 surface of the Si wafer substrates were cleaned by ultrasonication in acetone and methanol. The cleaned substrates were dried under nitrogen flow and then subjected to UV-ozone cleaning at 110 ^oC for 20 min. The substrates were then kept in desiccators with a few drops of OTS. The desiccators were evacuated for 3min and placed in an oven at 110 ^oC for 3 hr. After OTS treatment, the substrates were rinsed thoroughly with isopropanol and dried under nitrogen flow. The semiconductor layer were spin coated on the OTS treated Si/SiO_2 substrates from $TII(BFu)_2$ and $TII(Na)_2$ chloroform solution (5 mg mL^{-1}) at 1500 rpm for 60 s, and then annealed at various temperatures (ranging from 110 to 170 ^oC) for 10 min. Finally, gold (Au) source and drain electrodes (ca. 100 nm) were deposited on top of the semiconductor layers through shadow masks. For a typical OFET device reported here, the source-drain channel width (W) and channel length (L) were 8800 μm and 80 μm, respectively. OFET devices were characterized under an ambient environment using a Keithley 4200 parameter analyzer. The field effect mobility ($\mu_{sat.}$) was calculated from the saturation regime of the transfer characteristics from the following equation: $I_{DS} = \mu(WC_i/2L)(V_G-V_T)^2$. Atomic force microscopic (AFM) images of the thin films on OFETs were obtained by using an SII Nanonavi SPA-400 scanning probe microscope with an SII SI-DF40 cantilever.

Photovoltaic cells. OPV devices were fabricated on ITO glass substrates with a configuration of ITO/PEDOT:PSS/$TII(BFu)_2$ or $TII(Na)_2$:$PC_{71}BM$/Al. The ITO glass substrates were cleaned by sonification in acetone, deionized water, and isopropyl alcohol and dried in a nitrogen stream, followed by an UV-ozone treatment. Then a hole transport thin layer (~40 nm) of PEDOT:PSS was spin-cast on the substrates at 1500 rpm and annealed at 140 ^oC for 10 min on a hot plate under nitrogen. The active layer $TII(BFu)_2$ or $TII(Na)_2$:$PC_{71}BM$ was deposited by spin-casting chloroform solution (total concentration, 10 mg mL^{-1}) at 2500 rpm for 30 s in dry box and thermally annealed at 130 ^oC for 10 min. Subsequently, the aluminum cathode (90 nm) was thermally evaporated onto the active layer through a shadow mask under a pressure (<10^{-4} Pa). The effective device area was defined as 12 mm^2. The current density-voltage (J-V) characteristics were measured using a Keithley 2400 source meter under a simulated AM 1.5G conditions.

N-(1-dodecyl)thiophen-3-amine 2

3-bromothiophene (5.0 g, 30.67 mmol), dodecylamine (8.53 g, 46.01 mmol), copper (0.097 g, 1.53 mmol), copper(I) iodide (0.291 g, 1.53 mmol) and Potassium phosphate tribasic (13.02 g, 61.34 mmol) were stirred in 50 mL of dimethyl ethanolamine at 85 ^oC for 48 h under an N_2 atmosphere. After completion, ethyl acetate(200 mL) was added and the mixture is filtered. The organic layer was washed with water(3×50 mL), brine(50 mL) and dried over $MgSO_4$. After removal of solvent, The crude product was purified by chromatography on silica gel using hexane: EtOAc. Yield of N-(1-dodecyl)thiophen-3-amine (2) was about 41.3%. ^1H NMR (300 MHz, $CDCl_3$): δ/ppm: 7.15 (dd, 1H), 6.62 (d, 1H), 5.96 (s, 1H), 3.09 (t, 2H), 1.63 (dd, 2H), 1.47–1.22 (m, 18H), 0.92 (t, 3H).^{13}C NMR ($CDCl_3$): δ/ppm: 148.84, 124.90, 119.82, 95.14, 46.35, 31.88, 29.62, 29.59, 29.57, 29.44, 29.31, 27.18, 22.64, 14.06. TOF MS ES+(m/e): 268.20(M^+, 100%).

4-(1-dodecyl)-4H-thieno [3,2-b] pyrrole-5,6-dione 3

Compound **2** (3.30 g, 12.34 mmol) in 20 mL of CH_2Cl_2 was added dropwise to oxalyl dichloride (1.96 g, 15.43 mmol) in 10 mL of CH_2Cl_2 at 0 ^oC. After 0.5 h, triethylamine (2.25 g, 22.21 mmol) in 10

mL of CH_2Cl_2 was added dropwise and stirred 8 h at room temperature. Solvents were removed under vacuum and crude product was purified by chromatography on silica gel in hexane: CH_2Cl_2 mixture. 4-(1-dodecyl)-4H-thieno [3,2-b] pyrrole-5,6-dione (3) was obtained as orange powder in 68.1% yield. 1H NMR (300 MHz, $CDCl_3$): δ/ppm: 7.99 (d, 1H), 6.78 (d, 1H), 3.65 (t, 2H), 1.66 (dd, 2H), 1.40-1.15 (m, 18H), 0.88 (t, 3H). ^{13}C NMR ($CDCl_3$): δ/ppm: 173.02, 165.13, 161.44, 143.74, 121.04, 112.91, 42.14, 31.87, 29.66, 29.56, 29.49, 29.41, 29.29, 29.13, 28.15, 26.74, 22.64, 14.07. TOF MS ES+(*m/e*): 322.18 (M^+, 100%).

(E)-4,4'-bis(1-dodecyl)-[6,6'-bithieno[3,2-b]pyrrolylidene]-5,5'(4H,4'H)-dione 4

A solution of compound **3** (2.50 g, 7.78 mmol) and Lawesson's Reagent (1.61 g, 3.97 mmol) in 50 mL toluene were stirred at 65 °C for 5 h. The reaction mixture was then cooled down to room temperature. After removal of solvent, the crude product was purified twice by chromatography on silica gel in hexane : CH_2Cl_2 mixture. Yield 34.4%. ^1H NMR (300 MHz, $CDCl_3$): δ/ppm: 7.53 (d, 2H), 6.81 (d, 2H), 3.80 (t, 4H), 1.72 (dd, 4H), 1.38-1.17 (d, 36H), 0.87 (t, 6H). ^{13}C NMR ($CDCl_3$): δ/ppm: 170.99, 151.24, 134.33, 121.13, 114.21, 111.17, 41.80, 31.90, 29.68, 29.59, 29.53, 29.47, 29.31, 29.26, 28.58, 26.90, 22.67, 14.09. TOF MS ES+(*m/e*): 611.36 (M^+, 100%).

(E)-2,2'-dibromo-4,4'-bis(1-dodecyl)-[6,6'-bithieno[3,2-b]pyrrolylidene]-5,5'(4H,4'H)-dione 5

To an ice cold solution of compound **4** (0.7 g, 1.15 mmol) in 20 mL THF was added N-bromosuccimide (0.51 g, 2.88 mmol). The reaction progress was monitored by TLC. After completion, reaction was quenched by addition of water (20 mL), dichloromethane (50 mL) was added and organic layer separated. The organic layer was washed with water (3×15 mL), brine (15 mL) and dried over $MgSO_4$. After removal of solvent, the crude product was purified by chromatography on silica gel using hexane and DCM as eluent. Yield 78.7%. ^1H NMR (500 MHz, $CDCl_3$) δ/ppm: 6.85 (s, 2H), 3.74 (t, 4H), 1.73 – 1.65 (m, 4H), 1.38 – 1.20 (m, 36H), 0.88 (t, 6H). MALDI-TOF m/z: 768.18 (M^+, 100%).

(E)-2,2'-bis(benzofuran-2-yl)-4,4'-bis(1-dodecyl)-[6,6'-bithieno[3,2-b]pyrrolylidene]-5,5'(4H,4'H)-dione (TII(BFu)$_2$)

$Pd(PPh_3)_4$ (46 mg, 0.04 mmol) was added to a mixture of compound **5** (0.30 g, 0.39 mmol) and benzofuran-2-boronic acid (0.19 g, 1.17 mmol) in toluene (25 mL), ethanol (4 mL) and aqueous K_2CO_3 solution (2 M, 2 mL) under N_2. After the reaction was heated overnight at 90 °C, the solvent was evaporated. The residue was treated with water and extracted with CH_2Cl_2. The organic layer was separated, dried over anhydrous Mg_2SO_4, filtered and then concentrated. The crude product was purified by column chromatography using hexane and CH_2Cl_2 as eluent to afford a deep voilet solid in 69.2% yield (0.23 g). ^1H NMR (500 MHz, $CDCl_3$) δ 7.60 (d, 2H), 7.50 (d, 2H), 7.36-7.30 (m, 4H), 7.21 (s, 2H), 7.08 (s, 2H), 3.89 (m, 4H), 1.86 – 1.77 (m, 4H), 1.36-1.20 (m, 36H), 0.88 (t, 6H). Anal. Calcd. for $C_{52}H_{62}N_2O_4S_2$: C, 74.07; H, 7.41; N, 3.32. Found: C, 73.95; H, 7.51; N, 3.25. HRMS (ESI): (M^+, $C_{52}H_{62}N_2O_4S_2$), calcd: 842.4151; found: 842.4066.

(E)-2,2'-bis(2-naphthyl)-4,4'-bis(1-dodecyl)-[6,6'-bithieno[3,2-b]pyrrolylidene]-5,5'(4H,4'H)-dione (TII(Na)$_2$)

Prepared according to the procedure of TII(BFu)$_2$ using 2-naphthyl boronic acid instead. Yield: 74.6% (0.25g). ^1H NMR (500 MHz, $CDCl_3$) δ 8.22 (s, 2H), 7.87-7.82 (m, 8H), 7.55 – 7.45 (m, 4H), 7.17 (s, 2H), 3.89-3.86 (m, 4H), 1.85 – 1.75 (m, 4H), 1.33-1.18 (m, 36H), 0.85 (t, 6H). Anal. Calcd. for $C_{56}H_{66}N_2O_2S_2$: C, 77.91; H, 7.71; N, 3.25. Found: C, 77.34; H, 7.86; N, 3.03. HRMS (ESI): (M^+, $C_{56}H_{66}N_2O_2S_2$), calcd: 862.4566; found: 862.4454.

Acknowledgements

This research was supported by National Natural Science Foundation of China (no. 21304018) and Jiangsu Provincial Natural Science Foundation of China (no. BK20130619).

References

1 C. Wang; H. Dong; W. Hu; Y. Liu; D. Zhu, *Chem. Rev.*, 2012, 112, 2208.
2 J. G. Mei; Y. Diao; A. L. Appleton; L. Fang; Z. N. Bao, *J. Am. Chem. Soc.*, 2013, 135, 6724.
3 H. Sirringhaus, *Adv. Mater.*, 2014, 26, 1319.
4 A. Mishra; P. Baeuerle, *Angew. Chem. Int. Edit.*, 2012, 51, 2020.
5 Y. Lin; Y. Li; X. Zhan, *Chem. Soc. Rev.*, 2012, 41, 4245.
6 G. Li; R. Zhu; Y. Yang, *Nat. Photonics*, 2012, 6, 153.
7 Y. Li; P. Sonar; L. Murphy; W. Hong, *Energ. Environ. Sci.*, 2013, 6, 1684.
8 Y. C. Mei; M. A. Loth; M. Payne; W. M. Zhang; J. Smith; C. S. Day; S. R. Parkin; M. Heeney; I. McCulloch; T. D. Anthopoulos; J. E. Anthony; O. D. Jurchescu, *Adv. Mater.*, 2013, 25, 4352.
9 R. Hofmockel; U. Zschieschang; U. Kraft; R. Roedel; N. H. Hansen; M. Stolte; F. Wuerthner; K. Takimiya; K. Kern; J. Pflaum; H. Klauk, *Org. Electron.*, 2013, 14, 3213.
10 A. K. K. Kyaw; D. H. Wang; V. Gupta; J. Zhang; S. Chand; G. C. Bazan; A. J. Heeger, *Adv. Mater.*, 2013, 25, 2397.
11 J. Zhou; Y. Zuo; X. Wan; G. Long; Q. Zhang; W. Ni; Y. Liu; Z. Li; G. He; C. Li; B. Kan; M. Li; Y. Chen, *J. Am. Chem. Soc.*, 2013, 135, 8484.
12 W. L. Tang; D. Z. Huang; C. He; Y. P. Yi; J. Zhang; C. A. Di; Z. J. Zhang; Y. F. Li, *Org. Electron.*, 2014, 15, 1155.
13 Q. Zhang; B. Kan; F. Liu; G. K. Long; X. J. Wan; X. Q. Chen; Y. Zuo; W. Ni; H. J. Zhang; M. M. Li; Z. C. Hu; F. Huang; Y. Cao; Z. Q. Liang; M. T. Zhang; T. P. Russell; Y. S. Chen, *Nat. Photonics*, 2015, 9, 35.
14 B. Walker; A. B. Tomayo; X. D. Dang; P. Zalar; J. H. Seo; A. Garcia; M. Tantiwiwat; T. Q. Nguyen, *Adv. Funct. Mater.*, 2009, 19, 3063.
15 O. P. Lee; A. T. Yiu; P. M. Beaujuge; C. H. Woo; T. W. Holcombe; J. E. Millstone; J. D. Douglas; M. S. Chen; J. M. J. Frechet, *Adv. Mater.*, 2011, 23, 5359.
16 R. Zhou; Q.-D. Li; X.-C. Li; S.-M. Lu; L.-P. Wang; C.-H. Zhang; J. Huang; P. Chen; F. Li; X.-H. Zhu; W. C. H. Choy; J. Peng; Y. Cao; X. Gong, *Dyes Pigm.*, 2014, 101, 51.
17 W. Elsawy; C.-L. Lee; S. Cho; S.-H. Oh; S.-H. Moon; A. Elbarbary; J.-S. Lee, *Phys. Chem. Chem. Phys.*, 2013, 15, 15193.
18 A. Yassin; P. Leriche; M. Allain; J. Roncali, *New J. Chem.*, 2013, 37, 502.
19 R. S. Ashraf; A. J. Kronemeijer; D. I. James; H. Sirringhaus; I. McCulloch, *Chem. Commun.*, 2012, 48, 3939.
20 G. W. P. Van Pruissen; F. Gholamrezaie; M. M. Wienk; R. A. J. Janssen, *J. Mater. Chem.*, 2012, 22, 20387.

21 G. K. Dutta; A. R. Han; J. Lee; Y. Kim; J. H. Oh; C. Yang, *Adv. Funct. Mater.*, 2013, 23, 5317.
22 Y. Koizumi; M. Ide; A. Saeki; C. Vijayakumar; B. Balan; M. Kawamoto; S. Seki, *Polym. Chem.*, 2013, 4, 484.
23 T. Odajima; M. Ashizawa; Y. Konosu; H. Matsumoto; T. Mori, *J. Mater. Chem. C*, 2014, 2, 10455.
24 G. Kim; S.-J. Kang; G. K. Dutta; Y.-K. Han; T. J. Shin; Y.-Y. Noh; C. Yang, *J. Am. Chem. Soc.*, 2014, 136, 9477.
25 N. Berube; V. Gosselin; J. Gaudreau; M. Cote, *J. Phys. Chem. C*, 2013, 117, 7964.
26 Gaussian 03 (Revision B.05). Wallingford CT: Gaussian, Inc.; 2004,